ORIGINAL ARTICLE

Development of a novel animal model of lumbar vertebral endplate lesion by intervertebral disk injection of monosodium iodoacetate in rats

Toshiaki Maruyama[1] · Toshio Nakamae[1] · Naosuke Kamei[1] · Taiki Morisako[2] · Kazuto Nakao[1] · Fadlyansyah Farid[1,3] · Hiroki Fukui[1] · Nobuo Adachi[1]

© The Author(s) 2024

Abstract
Purpose Vertebral endplate lesions (EPLs) caused by severe disk degeneration are associated with low back pain. However, its pathophysiology remains unclear. In this study, we aimed to develop a vertebral EPL rat model mimicking severe intervertebral disk (IVD) degeneration by injecting monosodium iodoacetate (MIA) into the IVDs and evaluating it by assessing pain-related behavior, micro-computed tomography (CT) findings, and histological changes.
Methods MIA was injected into the L4-5 and L5-6 IVDs of Sprague–Dawley rats. Their behavior was examined by measuring the total distance traveled and the total number of rearing in an open square arena. Bone alterations and volume around the vertebral endplate were assessed using micro-CT. Safranin-O staining, immunohistochemistry, and tartrate-resistant acid phosphatase (TRAP) staining were performed for histological assessment.
Results The total distance and number of rearing times in the open field were significantly reduced in a time-dependent manner. Micro-CT revealed intervertebral osteophytes and irregularities in the endplates at 12 weeks. The bone volume/tissue volume (BV/TV) around the endplates significantly increased from 6 weeks onward. Safranin-O staining revealed severe degeneration of IVDs and endplate disorders in a dose- and time-dependent manner. Calcitonin gene-related peptide-positive nerve fibers significantly increased from 6 weeks onward. However, the number of osteoclasts decreased over time.
Conclusion Our rat EPL model showed progressive morphological vertebral endplate changes in a time- and concentration-dependent manner, similar to the degenerative changes in human IVDs. This model can be used as an animal model of severe IVD degeneration to better understand the pathophysiology of EPL.

Keywords Low back pain · Vertebral endplate lesion · Animal model · Monosodium iodoacetate · Osteoclasts

Introduction

Low back pain (LBP) is one of the most common health problems experienced by approximately 80% of the general population [1]. Suzuki et al. [2] identified that 78% of LBP cases were classified as specific LBP and that degenerative disk disease was a major risk factor for LBP. A previous study showed that Modic changes, which are endplate signal changes on magnetic resonance imaging (MRI), are associated with LBP [3]. Nakamae et al. [4] reported that bone marrow edema around the vertebral endplate on fat-saturated T2-weighted MRI was strongly associated with LBP. Thus, vertebral endplate lesions (EPLs) may be a clinical factor of LBP.

However, the pathophysiology of EPL remains unclear. Although animal models focusing on intervertebral disks (IVDs) have been developed [5], only a few models have focused on the vertebral endplates, which have reported that the changes around the vertebral endplates were not severe [6, 7]. Wang et al. reported a rat model where surgically-induced endplate microfracture caused IVD degeneration,

✉ Toshio Nakamae
toshinakamae623813@yahoo.co.jp

1 Department of Orthopaedic Surgery, Graduate School of Biomedical and Health Sciences, Hiroshima University, 1-2-3 Kasumi, Minami-Ku, HiroshimaHiroshima 734-8551, Japan

2 Department of Orthopaedic Surgery, Miyoshi Central Hospital, Hiroshima, Japan

3 Department of Orthopaedic and Traumatology, Faculty of Medicine, Hasanuddin University, Makassar, Indonesia

vertebral remodeling, and spinal cord sensitization [8]. Morisako et al. [9] developed an EPL model by resecting the IVDs. However, controlling the degree of EPL in these models was an arduous task. Therefore, we aimed to investigate severe IVD degeneration and EPL with controllable severity.

Monosodium iodoacetate (MIA) inhibits glyceraldehyde-3-phosphate dehydrogenase activity in chondrocytes, resulting in cell death and apoptosis [10]. Intra-articular injection of MIA is commonly used in animal models to induce morphological and histological changes in articular cartilage, similar to the changes observed in human osteoarthritis [11]. IVDs are cartilage-based structures that resemble the articular cartilage in terms of biochemical and cellular composition [12]. IVD degeneration and osteoarthritis of the articular cartilage are characterized by joint space narrowing, cartilage thinning, development of osteophytes, and subchondral sclerosis [13]. Recently, Suh et al. [14] reported that MIA injection into rat IVDs induced severe degenerative changes and also affected the pain behavior.

Hence, we hypothesized that MIA injection into rat IVDs would induce severe degenerative changes, resulting in EPL. In this study, we aimed to develop and investigate a rat model of vertebral EPL that mimics severe IVD degeneration and evaluate it by assessing the rat behavior, microcomputed tomography (CT), and histological findings.

Material and methods

Ethical considerations

This study was performed in accordance with the Guide for Animal Experimentation and was approved by the Committee of Research Facilities for Laboratory Animal Science (Graduate School of Biomedical & Health Sciences, Hiroshima University, Hiroshima, Japan).

Animals and surgery

A total of 72 Sprague–Dawley female rats aged 12 weeks were used in this study. During the experiment, the animals were housed in a standard 12-h light/dark cycle room with free access to food and water. Surgical procedures were performed on rats under isoflurane inhalation anesthesia. In supine position, the anterior part of the L3-4, L4-5, and L5-6 disks was exposed using a transperitoneal approach. Normal saline (0.9% NaCl w/v), 0.5 or 1 mg MIA (Sigma-Aldrich, St. Louis, MO, USA) (5 µl), was injected into the L4-5 and L5-6 IVDs of the rats using a Hamilton syringe with a 27G needle into the center of nucleus pulposus not to injure the cartilage endplate at a depth of 3.0 mm guided by a needle stopper. After injection, the surface of the disk was washed with 10 ml of saline. All the rats recovered from the surgery without any adverse events and were returned

to their cages. L3-4 disk, only exposure and not injected anything was defined as sham. All the behavioral tests were performed before surgery and 3, 6, 8, and 12 weeks after the surgery. In each group, eight rats were sacrificed at 3, 6, and 12 weeks after the surgery.

Behavioral tests

The open-field test was performed twice for each rat in a square arena (100 cm long, 100 cm wide, and 60 cm high) just before surgery and at each time point to assess pain-related behavior, in accordance with a previous study [15]. All tests were performed between 7 and 12 PM. Each rat was placed at a corner of the testing arena and allowed to freely explore the arena. The movements of the rats were monitored and recorded for 6 min. The total distance traveled by the rat in the arena and the number of rearing times getting up by hind legs were calculated using specific devices (SMART, Panlab SL, Barcelona, Spain). The total distance was assessed by calculating the variation between each period and before surgery. All post-injury data were analyzed as percentage change from pre-injury values.

Micro-computed Tomography

The bone volume fraction of the vertebral endplate was analyzed using high-resolution micro-CT (Skyscan 1176, Burker BioSpin) at 114-µA scanning intensity and 250-ms integration time. The rats were sacrificed, and the spine from thoracic to sacral region was removed, fixed, and placed in micro-CT for imaging at 3, 6, and 12 weeks after surgery. The micro-CT imaged the vertebral body every 0.3°, with a complete rotation of over 360°. Shooting one slice required approximately 1.156 s. Cross-sectional images were reconstructed using N Recon, a system within Skyscan 1176 with a slice width of 8.75 µm. The sagittal plane of the spine was used for evaluation. Bone volume/tissue volume (BV/TV, %), trabecular thickness (Tb.Th, mm), and bone mineral density (BMD, g/cm^3) around the endplate were assessed within a width of 300 µm from the endplate (Fig. 1). In the sham models, we assessed the area around the endplate at the L3-4 level and in other models, we assessed the area around the endplate at the L4-5 and L5-6 level.

Histological analysis

The harvested spinal columns were fixed in 4% paraformaldehyde for 3 days at 4 °C, decalcified in 18.5% ethylenediaminetetraacetic acid for 1 week, and subsequently embedded in paraffin. Mid-sagittal sections of 5-µm thickness of the spinal column were stained using the Safranin-O Fast-Green technique. Histological changes in the IVD were analyzed using a scoring system for rat IVD [16]

Fig. 1 Bone volume/tissue volume (BV/TV, %), trabecular thickness (Tb.Th, mm), and bone mineral density (BMD, g/cm^3) around the endplate were assessed within a width of 300 μm from the endplate
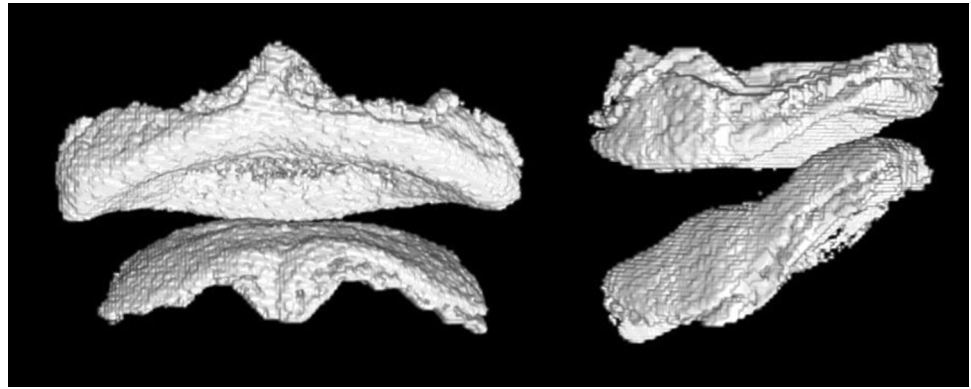
and in the vertebral endplates were scored using a grade of age-related histological changes in the endplate [17]. Disk height measurements were taken from the caudal aspect of the cartilaginous endplate to the cranial aspect of the cartilaginous endplate. For each image, an average of three measurements made from three areas of the disk space for one section from each rat: one from the anterior, one from the central, and one from the posterior side [18]. Disk height was analyzed as percentage change from sham models. Two spine surgeons who were blinded to the experiment assigned the scores for histological changes. Other sections were used for immunohistochemistry and tartrate-resistant acid phosphatase (TRAP) staining. TRAP staining was performed using a commercially available kit (Wako Pure Chemical Industries Ltd., Osaka, Japan) in accordance with the manufacturer's protocol. Six fields (200 × 200 μm each) around the vertebral endplate were randomly selected, and the number of TRAP-positive cells was counted using ImageJ (National Institution of Health). The number of TRAP-positive cells with multiple nuclei was also counted using ImageJ [19].

Immunohistochemical analysis

Each section was immunostained with a rabbit anti-calcitonin gene-related peptide (CGRP) antibody (1:500, ab139264, Abcam, Cambridge, UK) and chicken anti-68 kDa neurofilament-L (NF-L) antibody (1:500, ab72997, Abcam). Corresponding secondary antibodies were added to the sections and incubated in the dark for 1 hour. Secondary antibodies (1:500) used for CGRP and NF-L were Alexa Fluor 488-conjugated anti-rabbit IgG and Alexa Fluor 568-conjugated anti-chicken IgG. Sections were counterstained with 4',6-diamidino-2-phenylindole (DAPI) for immunofluorescence staining. Six fields (500 × 500 μm each) around the vertebral endplate were randomly selected, and ImageJ was used to calculate the percentage of the CGRP-positive region to the area of each field.

Statistical analysis

All results were expressed as mean and standard deviation. All data were analyzed using JMP® 15 software (SAS Institute Inc., Cary, NC, USA). The sham and the control disks were analyzed using the Mann–Whitney test. One-way analysis of variance (ANOVA) with Tukey–Kramer post-hoc test was used for multiple group comparisons. Statistical significance was set at $p < 0.05$.

Results

Behavioral testing

Compared to the control models, the MIA 0.5 mg and 1 mg injection models showed a significant reduction in the total distance and percentage change from pre-injury values traveled in the open-field test at 8 weeks after surgery, which continued up to 12 weeks (Fig. 2a, b). The MIA 0.5 mg injection models showed a significant reduction in the number of rearing times and percentage change from pre-injury values from 6 weeks, while the MIA 1 mg injection models showed a significant decrease in the number of rearing times and percentage change from pre-injury values from 3 weeks. This reduction in the number of rearing times continued in both the models up to 12 weeks. The number of rearing times decreased significantly at 3, 6, and 8 weeks in the MIA 1 mg injection models in comparison with the MIA 0.5 mg injection models. The number of rearing times percentage change from pre-injury values decreased significantly at 8 weeks in the MIA 1 mg injection models in comparison with the MIA 0.5 mg injection models (Fig. 2c, d).

Micro-CT findings

No obvious changes were observed in sham and control models at each week and either the MIA injection models at 3 weeks. However, at 6 weeks, erosion occurred at the
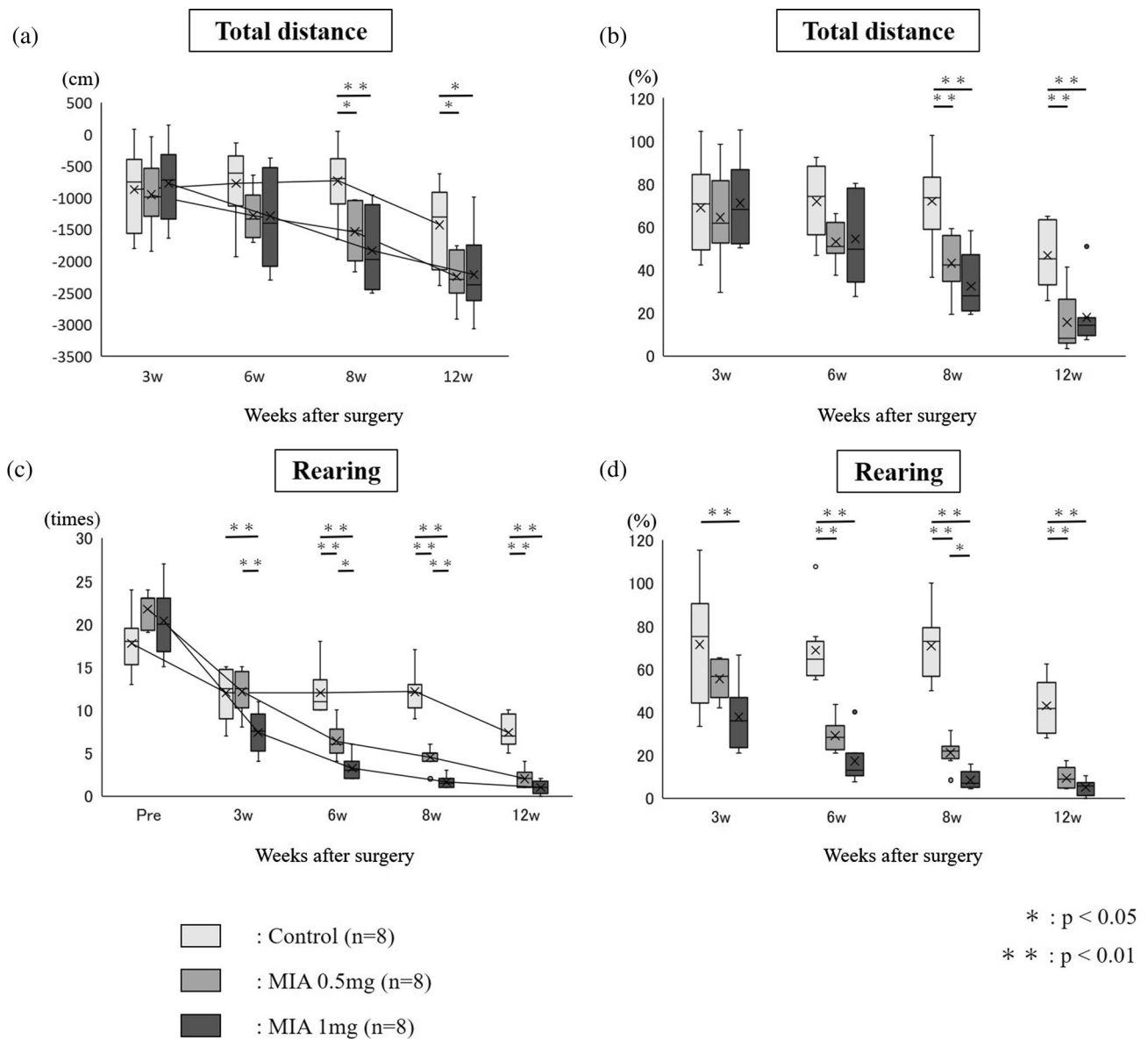
Fig. 2 Results of the open-field test: **a** total distance traveled and **b** percentage change from pre-injury values occurred. **c** The number of times rearing and **d** percentage change from pre-injury values

occurred. The total distance was assessed by calculating the variation between each period and before surgery

center of the vertebral endplates in both MIA 0.5 mg and 1 mg injection models. Furthermore, in the MIA 1 mg injection models, irregularities of the entire vertebral endplates and disappearance of the growth plates were observed. At 12 weeks, intervertebral osteophyte formation and irregularities of the endplates were observed in both the MIA injection models, with more irregularities being evident in the MIA 1 mg injection models (Fig. 3a, b). In the BV/TV, Tb. Th, and BMD, no obvious changes were observed between sham and control models at each week. In the MIA 0.5 mg and 1 mg injection models, the BV/TV, Tb. Th, and BMD increased significantly at 6 and 12 weeks compared

Fig. 3 a. **b** Micro-computed tomography findings of the intervertebral disks and endplates. At 6 weeks, erosion occurred at the center of the endplates in both monosodium iodoacetate (MIA) 0.5 mg and 1 mg injection models. Furthermore, in MIA 1 mg injection models, irregularities of the entire vertebral endplates and disappearance of the growth plates were observed. At 12 weeks, intervertebral osteophyte and irregularities of the endplates were observed in both MIA 0.5 mg and 1 mg injection models, with more irregularities evident in the endplates of the MIA 1 mg injection models. (**c**) The bone volume/tissue volume (BV/TV) ratio around the endplate. **d** The trabecular thickness (Tb.Th) around the endplate. **e** The bone mineral density (BMD) around the endplate
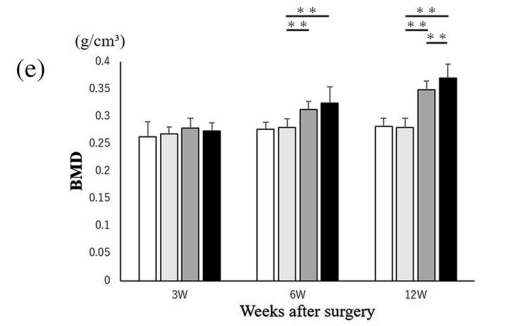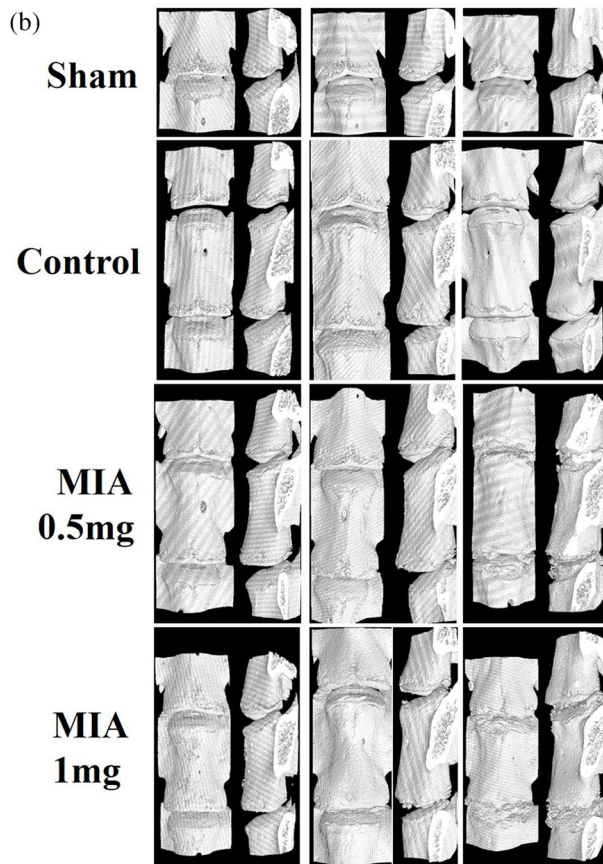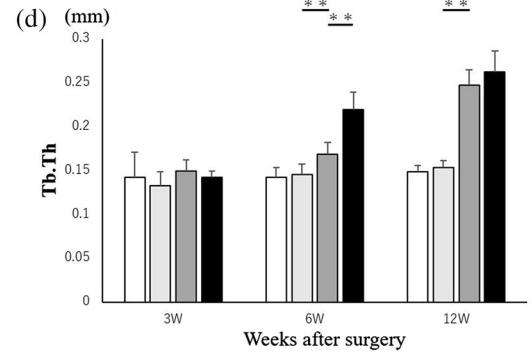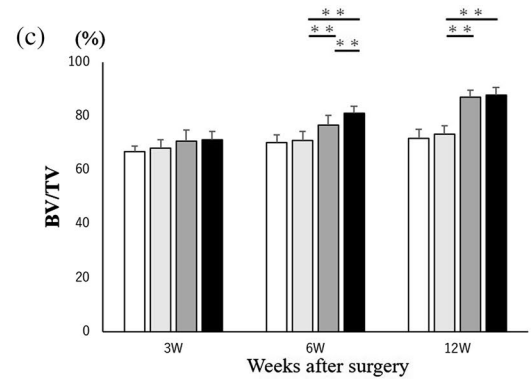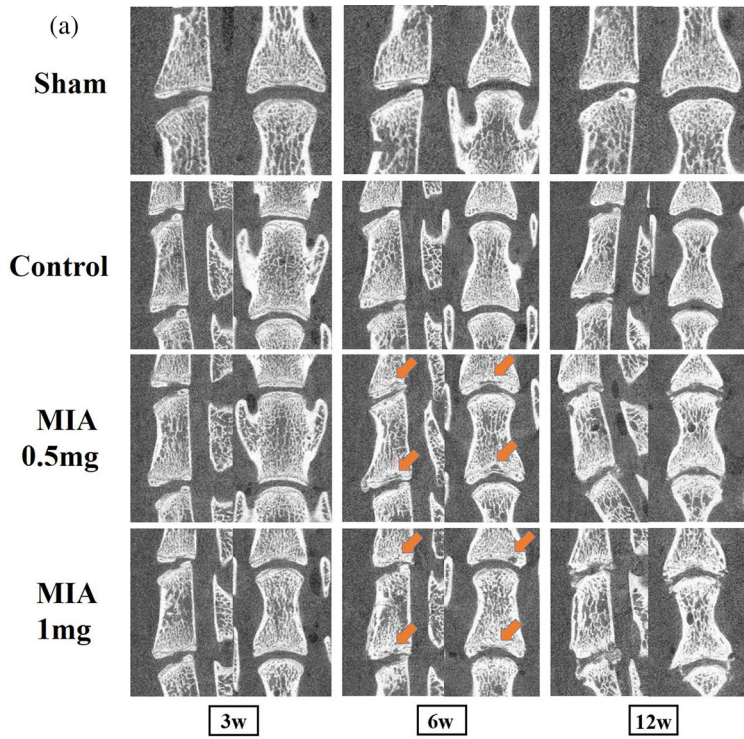
to the control models. The BV/TV and Tb. Th increased significantly at 6 weeks in the MIA 1 mg injection models in comparison with the MIA 0.5 mg injection models. The BMD increased significantly at 12 weeks in the MIA 1 mg injection models in comparison with the MIA 0.5 mg injection models (Fig. 3c, d, e).

Histological analysis

Safranin-O staining showed reduced disk height in the MIA injection models, with cracks and microfractures in the endplates and growth plates. At 6 weeks, disk degeneration progressed in the MIA 0.5 mg and 1 mg injection models, with more advanced cracks and microfractures. At 12 weeks, the disks and endplates showed a high degree of degeneration, and the disks were almost scarred. The cartilaginous endplates thinned considerably or were obliterated, with severe degeneration observed particularly in the MIA 1 mg injection models (Fig. 4a, b). The IVD scores were significantly higher in the control models than in the sham models at each week. In the endplate scores, no obvious changes were observed between sham and control models at each week. The IVD and endplate scores were significantly higher in the MIA injection models than in the control models at each week. The IVD score was significantly higher in the MIA 1 mg injection models than in the MIA 0.5 mg injection models at 3 weeks. Moreover, the endplate score was significantly higher in the MIA 1 mg injection models at 12 weeks (Fig. 4c, d). The disk height and percentage change from sham models were significantly higher in the MIA injection models than in the control models at each week. The disk height was significantly higher in the MIA 1 mg injection models than in the MIA 0.5 mg injection models at 3 and 6 weeks (Fig. 4e, f). In the total number of TRAP-positive cells and the number of TRAP-positive cells with multiple nuclei, no obvious changes were observed between sham and control models at each week. The total number of TRAP-positive cells and the number of TRAP-positive cells with multiple nuclei were significantly reduced in the MIA 1 mg injection models compared to the control models at 3 weeks, and it significantly decreased in the MIA 0.5 mg and 1 mg injection models at 6 and 12 weeks, respectively (Fig. 5a, b, c, d). Immunostaining for CGRP showed that the percentage of CGRP-positive areas around the vertebral endplate was significantly higher in the MIA 0.5 and 1 mg injection models than in the control models at 6 and 12 weeks. The percentage of CGRP-positive areas was significantly higher in the MIA 1 mg injection models compared to the MIA 0.5 mg injection models (Fig. 6a, b).

Discussion

Our study showed that MIA injection into the rat IVDs induced time- and concentration-dependent histological and structural degenerative changes in the IVDs and vertebral endplates. This model also demonstrated the pain-related behavioral patterns and increased expression of pain-related neuropeptides around the vertebral endplates.

Previous studies have reported that MIA induced in vivo and in vitro cartilage matrix degradation and chondrocyte apoptosis [20, 21]. Intra-articular injection of MIA has been reported to induce degenerative changes in the articular cartilage in a time- and concentration-dependent manner [22]. Suh et al. [14] injected MIA 0.4 mg and 4 mg into rat IVDs and assessed disk degeneration for up to 6 weeks. We also injected high-dose MIA (e.g., 1.5 and 3 mg) into the rat IVDs to develop severe IVD degeneration and EPL. However, the rats often died. Therefore, MIA 0.5 mg and 1 mg were selected for long-term observation in the current study.

In this study, we observed reduced disk height after MIA injection into the rat IVDs during each period. Disk height narrowing is an indicator of aging associated IVD degeneration [23]. In addition, IVD degeneration and endplate disorder progressed with increase in time and concentration. These results were consistent with the degeneration of human lumbar spine [24]. In particular, severe IVD degeneration and endplate disorder occurred 12 weeks after surgery in the MIA injection models. Long-term observations may induce more advanced IVD degeneration and EPL compared to the previous animal models [14].

The BV/TV, Tb.Th, and BMD around the endplate significantly increased in the MIA injection models from 6 weeks onward, suggesting osteosclerosis around the vertebral endplate. A previous study showed that severe disk degeneration and vertebral endplate osteosclerosis were associated with LBP [4]. Osteosclerosis may reflect the progression of IVD degeneration. In addition, we observed erosion at the center of the endplates at 6 weeks and intervertebral osteophytes at 12 weeks in the MIA injection models. Erosion at the center of the endplates suggests that the MIA had infiltrated around the vertebral endplates. Intervertebral osteophytes may reflect the process of spinal degeneration, often seen in IVD degeneration [25].

We focused on CGRP in the vertebral endplate because it plays an important role in bone metabolism and is a pain-related peptide [26]. CGRP has been reported to promote osteoblast proliferation and differentiation of bone marrow stromal cells for bone formation [27]. Our study showed that although the number of osteoclasts decreased over time in the MIA injection models, CGRP-positive nerve fibers significantly increased from 6 weeks onward. A previous study reported that CGRP-positive nerve fibers and the number of

Fig. 4 a, b Histopathological findings following Safranin-O fast green staining. Safranin-O staining showed reduced disk height in the monosodium iodoacetate (MIA) injection models, with cracks and microfractures in the endplates and growth plates. At 6 weeks, disk degeneration progressed in MIA 0.5 mg and 1 mg injection models, with more advanced cracks and microfractures. At 12 weeks, the disks and endplate tissue demonstrated a high degree of degeneration, and the disks were almost scarred. The cartilaginous endplates thinned considerably or were obliterated, with severe degeneration particularly observed in the MIA 1 mg injection models (a. Scale bars, 200 µm. b. Scale bars, 100 µm.) (**c, d**) The intervertebral disk (IVD) and endplate score were significantly higher in the MIA injection models compared to control models every week. The IVD score was significantly higher in the MIA 1 mg injection models than in the MIA 0.5 mg injection models at 3 weeks. Moreover, the endplate score was significantly higher in the MIA 1 mg injection models at 12 weeks. (**e, f**) The disk height and percentage change from sham models were significantly higher in the MIA injection models than in the control models at each week. The disk height was significantly higher in the MIA 1 mg injection models than in the MIA 0.5 mg injection models at 3 and 6 weeks
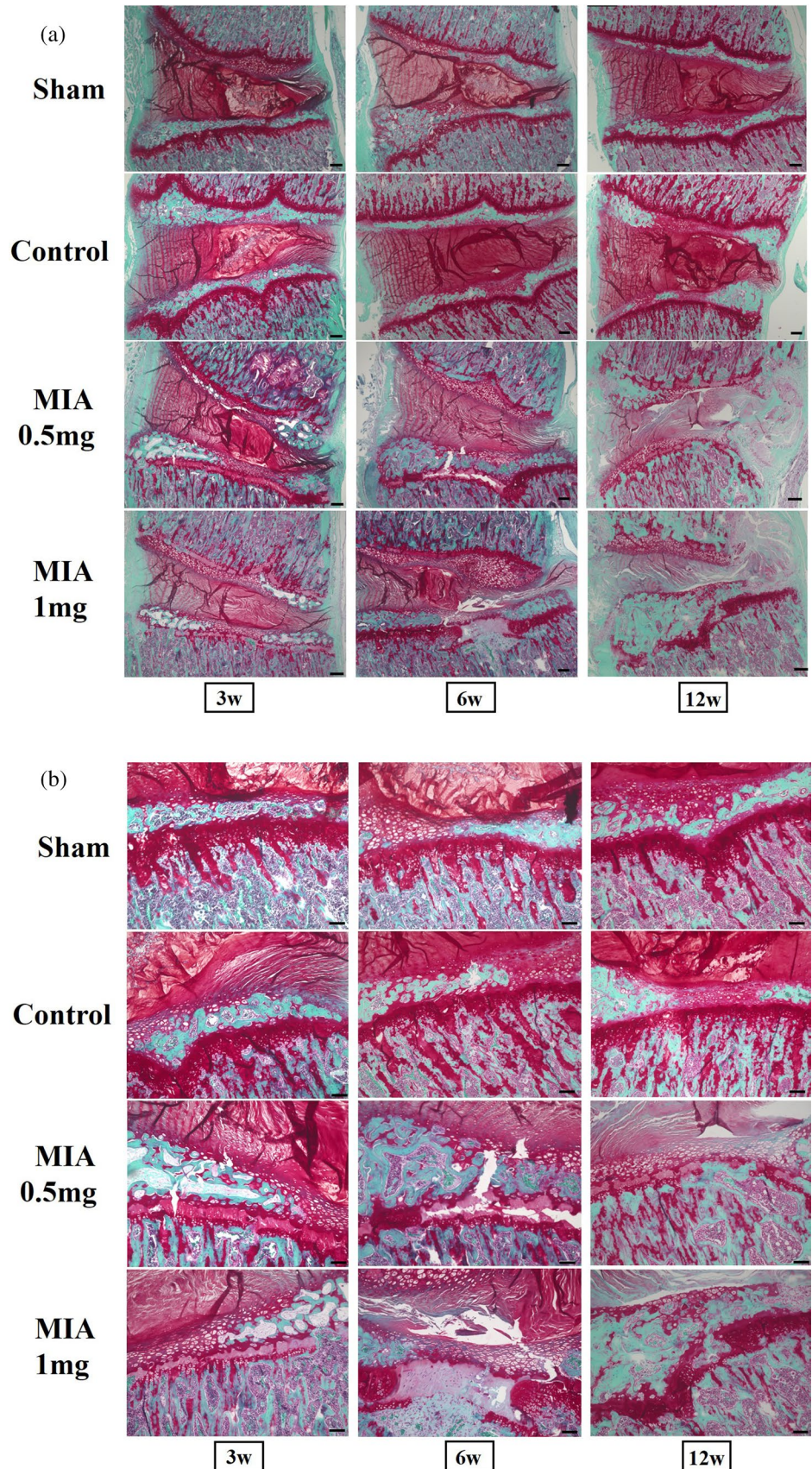
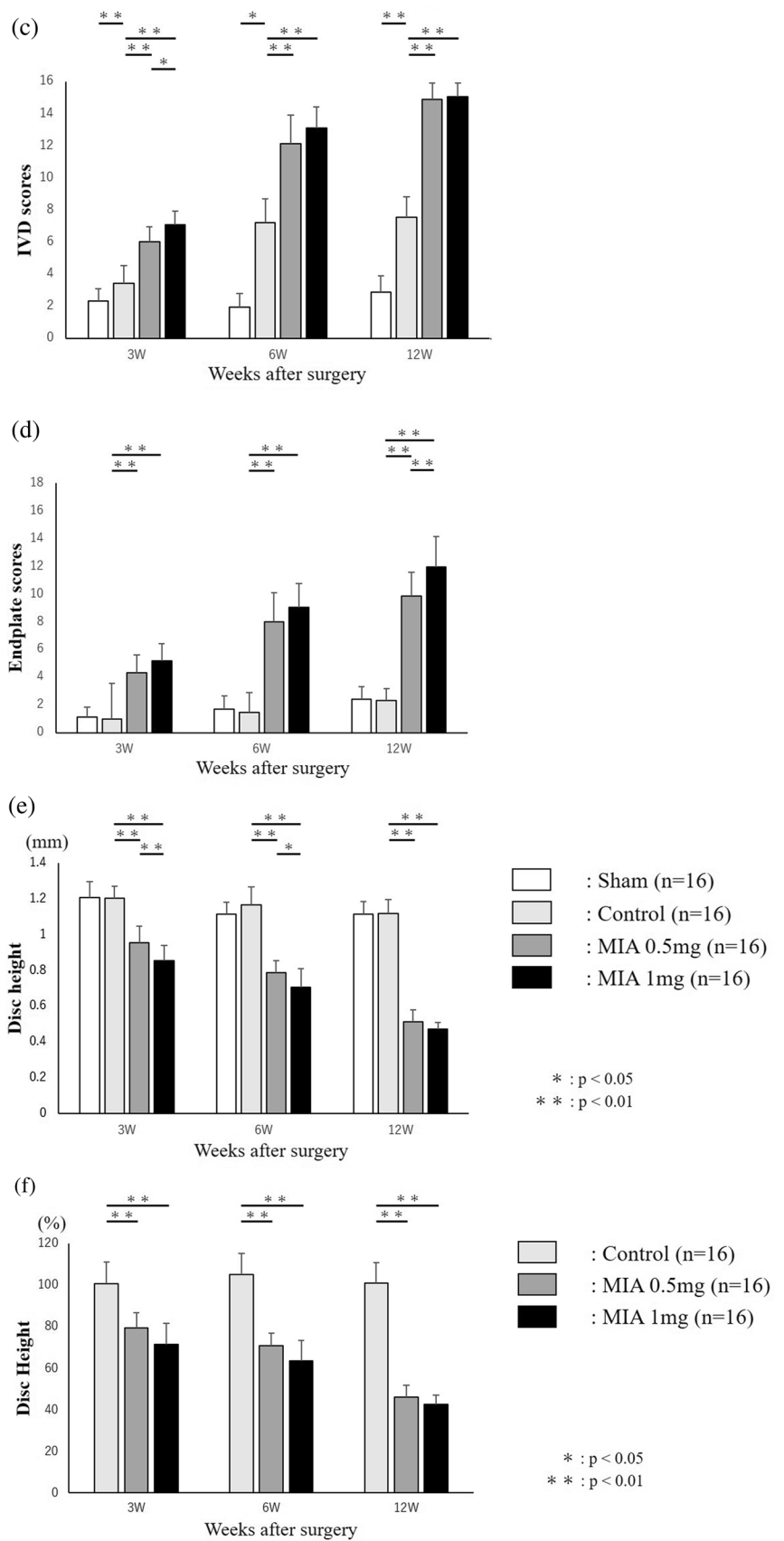**Fig. 4** (continued)

(c)

(d)

(e)

(f)

Fig. 5 Histological findings following tartrate-resistant acid phosphatase (TRAP) staining. **a** Weak magnification (scale bar, 200 μm) (**b**) strong magnification (scale bar, 100 μm). **c**, **d** In the total number of TRAP-positive cells and the number of TRAP-positive cells with multiple nuclei, no obvious changes were observed between sham and control models at each week. The total number of TRAP-positive cells and the number of TRAP-positive cells with multiple nuclei were significantly reduced in the MIA 1 mg injection models compared to the control models at 3 weeks, and it significantly decreased in the MIA 0.5 mg and 1 mg injection models at 6 and 12 weeks, respectively
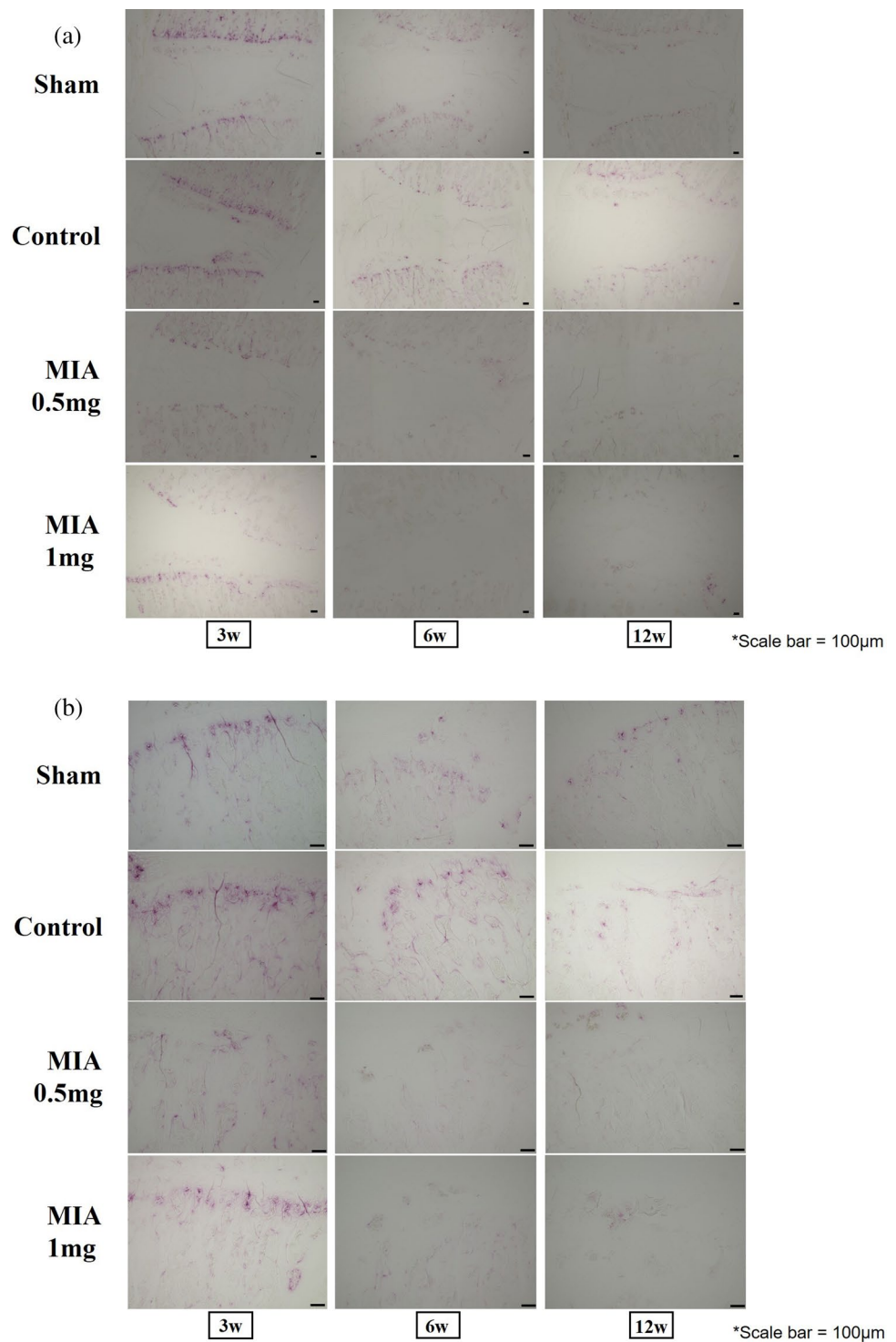
TRAP-positive cells in the subchondral bone were significantly higher than those in the control knee MIA injection rat model [28]. IVDs are similar to articular cartilage in cellular composition but differ in structure. Nutrients diffuse by gradient concentration from the capillary bed, through the cartilaginous endplate and dense disk matrix, to inner disk cells, while metabolic wastes move oppositely [29]. The differences in these results and structure suggest that after MIA injection into the IVDs, MIA infiltrates the EPL and induces TRAP-positive cell death. In this respect, MIA

Fig. 5 (continued)

(c)

(d)

☐ : Sham (n=12)
☐ : Control (n=12)
▨ : MIA 0.5mg (n=12)
■ : MIA 1mg (n=12)

∗ : p < 0.05
∗ ∗ : p < 0.01
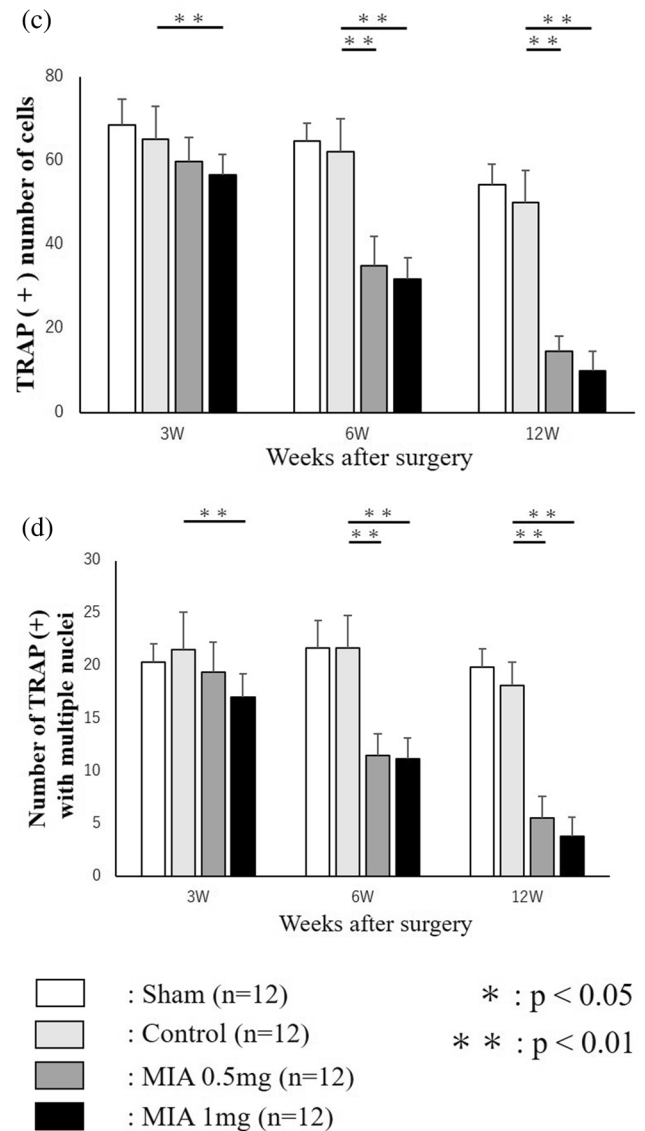
injection into the IVD model differed from the intra-articular injection model.

In both MIA models, the total distance was significantly reduced 8 weeks after surgery and was maintained until 12 weeks. Rearing time also significantly decreased from 6 weeks in MIA 0.5 mg injection models and after 3 weeks in MIA 1 mg injection models, which manifested more quickly than the reduction in total distance. Rearing has been reported to be more sensitive than the total distance observed in the knee MIA injection model in rats [15, 30]. Our results indicate that the lumbar spine is not loaded in the horizontal activity, whereas rearing involves weight distribution on the lumbar spine.

There are several limitations to this study. First, we used the rats aged 12 weeks that is skeletally-immature. We cannot deny the possibility that MIA might impact the growth plate and cartilage endplate instead of pure cartilage

endplate. Second, gender difference may affect the result of EPL. Third, the current model of MIA injection into the IVDs did not really mimic the clinical setting of vertebral endplate lesion. Further research is needed to clarify the influence of MIA injection into the rat IVDs.

Conclusion

The current study aimed to develop a vertebral EPL rat model mimicking severe IVD degeneration by injecting MIA into the IVDs and evaluating it by assessing pain-related behavior, micro-CT findings, and histology. This model showed progressive morphological EPL changes in a time- and concentration-dependent manner, similar to the degenerative changes in human IVDs. We observed significantly

Fig. 6 **a** Representative images of immunostaining of calcitonin gene-related peptide (CGRP) (green), neurofilament-L (NF-L) (red), and 4′,6-diamidino-2-phenylindole (DAPI) (blue) around the endplates (scale bars, 100 μm). **b** Immunostaining for CGRP showed that the percentage of CGRP-positive areas around the vertebral endplates was significantly higher in the monosodium iodoacetate (MIA) 0.5 and 1 mg injection models than in the control models at 6 and 12 weeks. The percentage of CGRP-positive areas was significantly higher in the MIA 1 mg injection models than in the MIA 0.5 mg injection models
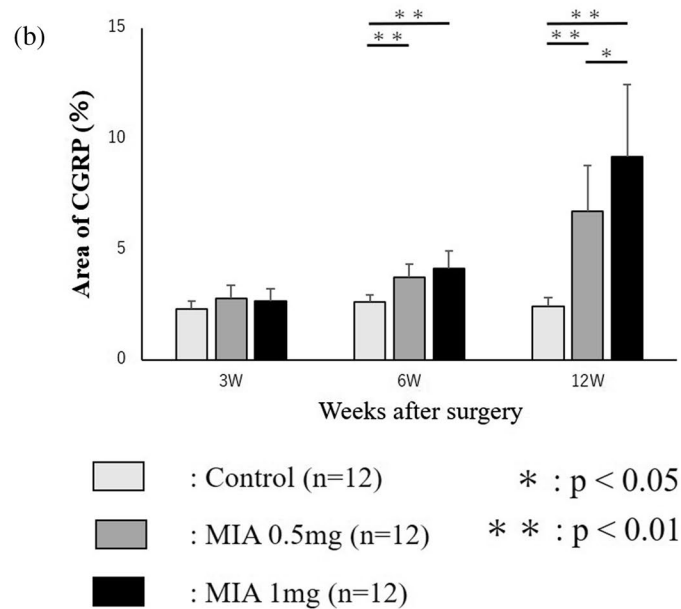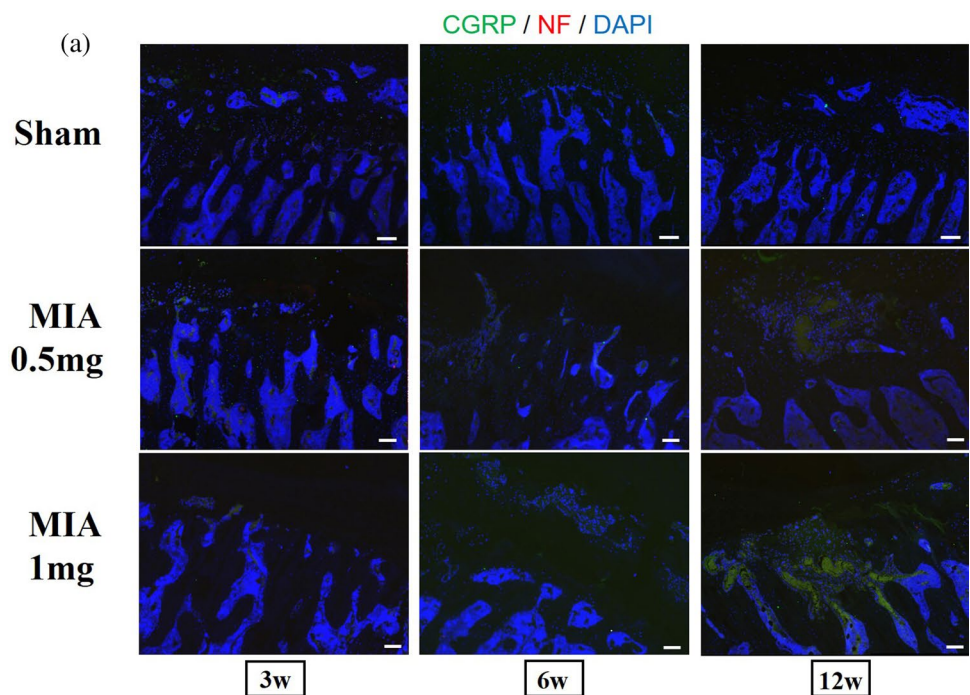
increased CGRP-positive nerve fibers around the vertebral endplate and pain-related behavior in MIA injection models. This model can be used as an animal model of severe IVD degeneration for better understanding of the pathophysiology of EPL and developing new treatment strategies involving bone metabolism.

Declarations

Conflict of interest The authors declare that they have no conflict of interest.

Ethical approval All experimental procedures were performed in accordance with the Guidelines for Animal Experimentation at Hiroshima University and with the approval of the Committee of Research Facilities for Laboratory Animal Sciences, Graduate School of Biomedical Sciences, Hiroshima University.

Open Access This article is licensed under a Creative Commons Attribution 4.0 International License, which permits use, sharing, adaptation, distribution and reproduction in any medium or format, as long as you give appropriate credit to the original author(s) and the source, provide a link to the Creative Commons licence, and indicate if changes were made. The images or other third party material in this article are included in the article's Creative Commons licence, unless indicated otherwise in a credit line to the material. If material is not included in the article's Creative Commons licence and your intended use is not permitted by statutory regulation or exceeds the permitted use, you will need to obtain permission directly from the copyright holder. To view a copy of this licence, visit http://creativecommons.org/licenses/by/4.0/.

References

1. Kirkaldy-Willis WH, Farfan HF (1982) Instability of the lumbar spine. Clin Orthop Relat Res 165:110–123 (**0**)
2. Suzuki H, Kanchiku T, Imajo Y, Yoshida Y, Nishida N, Taguchi T (2016) Diagnosis and characters of non-specific low back pain in japan: the yamaguchi low back pain study. PLoS ONE 11(8):e0160454. https://doi.org/10.1371/journal.pone.0160454
3. Rahme R, Moussa R (2008) The modic vertebral endplate and marrow changes: pathologic significance and relation to low back pain and segmental instability of the lumbar spine. AJNR Am J Neuroradiol 29(5):838–842. https://doi.org/10.3174/ajnr.A0925
4. Nakamae T, Yamada K, Shimbo T, Kanazawa T, Okuda T, Takata H, Hashimoto T, Hiramatsu T, Tanaka N, Ochi M, Olmarker K, Fujimoto Y (2016) Bone marrow edema and low back pain in elderly degenerative lumbar scoliosis: a cross-sectional study. Spine 41(10):885–892. https://doi.org/10.1097/BRS.0000000000001315
5. Fukui D, Kawakami M, Yoshida M, Nakao S, Matsuoka T, Yamada H (2015) Gait abnormality due to spinal instability after lumbar facetectomy in the rat. Eur Spine J 24(9):2085–2094. https://doi.org/10.1007/s00586-014-3537-y
6. Ni S, Ling Z, Wang X, Cao Y, Wu T, Deng R, Crane JL, Skolasky R, Demehri S, Zhen G, Jain A, Wu P, Pan D, Hu B, Lyu X, Li Y, Chen H, Qi H, Guan Y, Dong X, Wan M, Zou X, Lu H, Hu J, Cao X (2019) Sensory innervation in porous endplates by Netrin-1 from osteoclasts mediates PGE2-induced spinal hypersensitivity in mice. Nat Commun 10(1):5643. https://doi.org/10.1038/s41467-019-13476-9
7. Maerz T, Newton M, Marek AA, Planalp M, Baker K (2018) Dynamic adaptation of vertebral endplate and trabecular bone following annular injury in a rat model of degenerative disc disease. Spine J 18(11):2091–2101. https://doi.org/10.1016/j.spinee.2018.05.045
8. Wang D, Lai A, Gansau J, Seifert AC, Munitz J, Zaheer K, Bhadouria N, Lee Y, Nasser P, Laudier DM, Holguin N, Hecht AC, Iatridis JC (2023) Lumbar endplate microfracture injury induces Modic-like changes, intervertebral disc degeneration and spinal cord sensitization - an in vivo rat model. Spine J 23(9):1375–1388. https://doi.org/10.1016/j.spinee.2023.04.012
9. Morisako T, Nakamae T, Kamei N, Tamura T, Tsuchikawa Y, Harada T, Maruyama T, Adachi N (2022) Development of a rat model with lumbar vertebral endplate lesion. Eur Spine J 31(4):874–881. https://doi.org/10.1007/s00586-022-07148-4
10. Jiang L, Li L, Geng C, Gong D, Jiang L, Ishikawa N, Kajima K, Zhong L (2013) Monosodium iodoacetate induces apoptosis via the mitochondrial pathway involving ROS production and caspase activation in rat chondrocytes in vitro. J Orthop Res 31(3):364–369. https://doi.org/10.1002/jor.22250
11. Kuyinu EL, Narayanan G, Nair LS, Laurencin CT (2016) Animal models of osteoarthritis: classification, update, and measurement of outcomes. J Orthop Surg Res 2(11):19. https://doi.org/10.1186/s13018-016-0346-5
12. Gupta KB, Duryea J, Weissman BN (2004) Radiographic evaluation of osteoarthritis. Radiol Clin North Am 42(1):11–41. https://doi.org/10.1016/S0033-8389(03)00169-6
13. Pye SR, Reid DM, Lunt M, Adams JE, Silman AJ, O'Neill TW (2007) Lumbar disc degeneration: association between osteophytes, end-plate sclerosis and disc space narrowing. Ann Rheum Dis 66(3):330–333. https://doi.org/10.1136/ard.2006.052522
14. Suh HR, Cho HY, Han HC (2022) Development of a novel model of intervertebral disc degeneration by the intradiscal application of monosodium iodoacetate (MIA) in rat. Spine J 22(1):183–192. https://doi.org/10.1016/j.spinee.2021.06.008
15. Nagase H, Kumakura S, Shimada K (2012) Establishment of a novel objective and quantitative method to assess pain-related behavior in monosodium iodoacetate-induced osteoarthritis in rat knee. J Pharmacol Toxicol Methods 65(1):29–36. https://doi.org/10.1016/j.vascn.2011.10.002
16. Lai A, Gansau J, Gullbrand SE, Crowley J, Cunha C, Dudli S, Engiles JB, Fusellier M, Goncalves RM, Nakashima D, Okewunmi J, Pelletier M, Presciutti SM, Schol J, Takeoka Y, Yang S, Yurube T, Zhang Y, Iatridis JC (2021) Development of a standardized histopathology scoring system for intervertebral disc degeneration in rat models: An initiative of the ORS spine section. JOR Spine 4(2):e1150. https://doi.org/10.1002/jsp2.1150
17. Boos N, Weissbach S, Rohrbach H, Weiler C, Spratt KF, Nerlich AG (2002) Classification of age-related changes in lumbar intervertebral discs: 2002 Volvo Award in basic science. Spine (Phila Pa 1976) 27(23):2631–2644. https://doi.org/10.1097/00007632-200212010-00002
18. Mosekilde L, Danielsen CC, Knudsen UB (1993) The effect of aging and ovariectomy on the vertebral bone mass and biomechanical properties of mature rats. Bone 14(1):1–6. https://doi.org/10.1016/8756-3282(93)90248-9
19. Cornish J, Callon KE, Bava U, Kamona SA, Cooper GJ, Reid IR (2001) Effects of calcitonin, amylin, and calcitonin gene-related peptide on osteoclast development. Bone 29(2):162–168. https://doi.org/10.1016/s8756-3282(01)00494-x
20. Grossin L, Cournil-Henrionnet C, Pinzano A, Gaborit N, Dumas D, Etienne S, Stoltz JF, Terlain B, Netter P, Mir LM, Gillet P (2006) Gene transfer with HSP 70 in rat chondrocytes confers cytoprotection in vitro and during experimental osteoarthritis. FASEB J 20(1):65–75. https://doi.org/10.1096/fj.04-2889com
21. Wu W, Xu X, Dai Y, Xia L (2010) Therapeutic effect of the saponin fraction from Clematis chinensis Osbeck roots on osteoarthritis induced by monosodium iodoacetate through protecting articular cartilage. Phytother Res 24(4):538–546. https://doi.org/10.1002/ptr.2977
22. Udo M, Muneta T, Tsuji K, Ozeki N, Nakagawa Y, Ohara T, Saito R, Yanagisawa K, Koga H, Sekiya I (2016) Monoiodoacetic acid induces arthritis and synovitis in rats in a dose- and

time-dependent manner: proposed model-specific scoring systems. Osteoarthr Cartil 24(7):1284–1291. https://doi.org/10.1016/j.joca.2016.02.005

23. Akeda K, Yamada T, Inoue N, Nishimura A, Sudo A (2015) Risk factors for lumbar intervertebral disc height narrowing: a population-based longitudinal study in the elderly. BMC Musculoskelet Disord 9(16):344. https://doi.org/10.1186/s12891-015-0798-5

24. Vo NV, Hartman RA, Patil PR, Risbud MV, Kletsas D, Iatridis JC, Hoyland JA, Le Maitre CL, Sowa GA, Kang JD (2016) Molecular mechanisms of biological aging in intervertebral discs. J Orthop Res 34(8):1289–1306. https://doi.org/10.1002/jor.23195

25. Menkes CJ, Lane NE (2004) Are osteophytes good or bad? Osteoarthr Cartil 12:53–54. https://doi.org/10.1016/j.joca.2003.09.003

26. Sample SJ, Hao Z, Wilson AP, Muir P (2011) Role of calcitonin gene-related peptide in bone repair after cyclic fatigue loading. PLoS ONE 6(6):e20386. https://doi.org/10.1371/journal.pone.0020386

27. Villa I, Dal Fiume C, Maestroni A, Rubinacci A, Ravasi F, Guidobono F (2003) Human osteoblast-like cell proliferation induced by calcitonin-related peptides involves PKC activity. Am J Physiol Endocrinol Metab 284(3):E627–E633. https://doi.org/10.1152/ajpendo.00307.2002

28. Yu D, Liu F, Liu M, Zhao X, Wang X, Li Y, Mao Y, Zhu Z (2013) The inhibition of subchondral bone lesions significantly reversed the weight-bearing deficit and the overexpression of CGRP in DRG neurons, GFAP and Iba-1 in the spinal dorsal horn in the monosodium iodoacetate induced model of osteoarthritis pain. PLoS ONE 8(10):e77824. https://doi.org/10.1371/journal.pone.0077824

29. Huang YC, Urban JP, Luk KD (2014) Intervertebral disc regeneration: do nutrients lead the way? Nat Rev Rheumatol 10(9):561–566. https://doi.org/10.1038/nrrheum.2014.91

30. Gonçalves S, Hathway GJ, Woodhams SG, Chapman V, Bast T (2023) No evidence for cognitive impairment in an experimental rat model of knee osteoarthritis and associated chronic pain. J Pain S1526–5900(23):00393. https://doi.org/10.1016/j.jpain.2023.04.002